Available online at www.sciencedirect.com
ScienceDirect
Journal of Power Sources 169 (2007) 327–333
JOURNAL OF POWER SOURCES
www.elsevier.com/locate/jpowsour

Study of the synergism effect of a binary carbon system in the nanostructure of the gas diffusion electrode (GDE) of a proton exchange membrane fuel cell

Mehdi Kheirmand [a], Hussein Gharibi [a,b,*], Rasol Abdullah Mirzaie [c], Monireh Faraji [a], Mohammad Zhiani [a]

[a] *Department of Chemistry, Tarbiat Modarres University, P.O. Box 14155-4838, Tehran, Iran*
[b] *Iranian Information and Documentation Center (IRANDOC), Tehran, Iran*
[c] *Department of Chemistry, Faculty of Science, Shahid Rajaee University, Tehran, Iran*

Received 21 April 2006; received in revised form 12 February 2007; accepted 15 March 2007
Available online 30 March 2007

Abstract

We report on the use of dual carbon supports activated charcoal (AC) and Vulcan XC-72R (VC) as catalysts for the fabrication of a gas diffusion electrode. The electrocatalytic properties for the oxygen reduction reaction were evaluated in a sulfuric acid electrolyte using polarization curves and electrochemical impedance spectroscopy. The water uptake and oxygen permeability were also obtained, as were the performances of electrodes in a membrane electrode assembly. A binary support electrode exhibits better performance than the usual single support electrode, with the best performance being obtained when the mass ratio of the two carbons is 50:50.

Keywords: Binary carbon supports; Gas diffusion electrode; Proton exchange membrane fuel cell; Oxygen reduction reaction; Synergism effect; Fuel cell

1. Introduction

Polymer electrolyte membrane fuel cells (PEMFCs) are receiving increasing attention due to their high efficiency and environmentally friendly characteristics [1]. Their performance is mainly dependent on the structure and properties of the material used for the gas diffusion electrode (GDE) [1,2]. The type and properties of the carbon support, such as its hydrophobicity [3], surface area [4], electronic conductivity [5], and surface functional groups [6], all contribute to the overall performance of the GDE [7].

Carbon is not only used to conduct electrons in a GDE, but also should result in the presence of macro- and microscopic pores [8] and help to stabilize the three-phase boundary and morphology [7]. The importance of the atomic structure of the carbon support on catalytic activity and the effect of carbon support on the platinum work function have also been studied [9].

Various types of carbon and graphite, such as Vulcan [10], black pearl [11,12], acetylene black [11–13], Ketjen black carbon [13], Iranian carbon black [14], graphite nanofiber [3], carbon nanotube [15], high-surface-area carbon nanohorns [16], treated carbon blacks [17], and other materials such as ionic and electronic conductive polymers [18] and silicon carbide [19] have been applied as single supports in investigations of the oxygen reduction reaction (ORR) in GDEs. However, when using a single carbon support it may be difficult to obtain the optimum parameters needed for enhancing the gas diffusion performance of the ORR, and to obtain optimized ionic and electronic conductivity, and good morphology, surface area, electron diffusion, and product removal [7]. Sakaguchi et al. [20] and Watanabe et al. [21] first reported the use of binary carbon supports in liquid electrolyte fuel cells. Wang et al. [7] and Gharibi and Abdullah Mirzaie [22] reported the use of binary carbon supports with different surface areas. Huang et al. [23] recently used carbon nanotubes as secondary supports in an alkaline GDE, and obtained better electrochemical performance and improved

* Corresponding author at: Department of Chemistry, Tarbiat Modarres University, P.O. Box 14115 4838, Tehran 14155, Iran. Tel.: +98 21 66462548; fax: +98 21 66462254.
E-mail address: gharibi@irandoc.ac.ir (H. Gharibi).

0378-7753/$ – see front matter © 2007 Elsevier B.V. All rights reserved.
doi:10.1016/j.jpowsour.2007.03.053

utilization of platinum catalysts when using binary carbon supports.

In this work we used active charcoal (AC) and Vulcan XC-72R (VC) as catalyst supports in a GDE for PEMFCs at different mass ratios in order to determine the best mass ratio of these types of carbon. Each carbon type has advantages and disadvantages when used in isolation. The surface area of AC ($900\,m^2\,g^{-1}$) are higher than VC ($254\,m^2\,g^{-1}$) since the water removal of VC is better than AC. Also the particle size of AC (4 nm) is smaller than VC (30 nm). In the present study, GDEs have been fabricated in which the electrocatalyst consists of a mixture of two types of electrocatalyst with different surface areas. Specifically, a mixture of platinum on carbon with high and low surface area is used. Such mixtures provide an opportunity to improve the cell performance compared with that of cells with a single carbon substrate. We evaluated and characterized the optimal synergism effects through combining two types of carbon on the performance of a GDE by measuring polarization curves at different temperatures (from 298 to 333 K in 5-K steps) and performing electrochemical impedance spectroscopy (EIS) in a conventional three-electrode system. The performance of electrodes was also examined in single-cell fuel cell.

2. Experimental

2.1. Electrode preparation

The three-layer electrode was prepared by casting a 40 wt.% polytetrafluoroethylene and 60 wt.% active carbon Vulcan XC-72 slurry on a TGP-060H carbon paper (Electrochem), as detailed elsewhere [24]. The attained electrode was hot pressed and sintered. Catalyst inks were prepared by mixing a platinum-on-activated-charcoal (10 wt.%) catalyst (Pt/AC; Merck) and/or a platinum-on-Vulcan-XC-72 (10 wt.%) catalyst (Pt/V; E-Tek) in different mass ratios with Nafion solution (5 wt.%; Aldrich, with low-molecular-weight aliphatic alcohols) in isopropyl alcohol, distilled water, and glycerol [25]. The loadings of platinum and Nafion were 0.5 and 1 mg cm^{-2}, respectively. After spraying the catalyst ink on the diffusion layer, the electrodes were air dried at 353 K. The loading of the catalyst are controlled by weighing. Catalyst inks were prepared with five mass ratios using a content of Pt/V from 0 to 100 wt.% and that of Pt/AC in reverse (to ensure a constant total platinum loading of 0.5 mg cm^{-2}).

2.2. Membrane electrode assembly fabrication

Two similar electrode and a treated [26] Nafion-117 sheet were coupled into a single-cell membrane electrode assembly (MEA) by hot pressing at 395 K and 70 atm for 5 min. The MEA was then cooled at room temperature and placed in gold-coated stainless steel single-cell fuel cell for electrochemical testing.

2.3. Electrochemical measurements

The ORR was investigated at the GDE (geometric exposed area of 1 cm^2) in 0.5 M sulfuric acid (Merck).

The electrochemical measurements were performed at different temperatures in a conventional three-electrode system, with gas flowing along the back of the GDE. The GDE was mounted in a Teflon holder containing a graphite ring as the current collector and having the provision for an oxygen supply at the back of the electrode. A platinum flat electrode was used as a counter electrode, and an Ag/AgCl reference electrode was placed close to the working electrode surface using a Luggin capillary. The electrochemical cell was connected to a PC-controlled potentiostat–galvanostat (EG&G 273 A).

After pre-treating the GDE with Pt [26], slow-sweep voltammograms were recorded at eight temperatures (as mentioned in Section 1) oxygen purged solutions at a rate of 0.1 mV s^{-1} between 1 and −0.3 V relative to an Ag/AgCl electrode for an oxygen supply at the back of the electrode at a rate of 30 ml min^{-1}. To determine the charge associated with the active area and the electrochemical platinum surface area, cyclic voltammograms were recorded after cycling the electrodes until a stationary response was obtained, in an argon atmosphere. The cyclic voltammetry (CV) scan rate was 50 mV s^{-1} between −0.3 and 1.2 V relative to an Ag/AgCl reference electrode. The measurements were performed at various potentials that are cathodic to the equilibrium potential of the oxygen electrode. An ac potential of 5 mV was superimposed on the dc potential, and the impedance spectra were collected for frequencies between 10 kHz and 0.1 Hz.

Chronoamperograms were obtained by holding the potential of the GDE at 1 V for 20 s and then stepping it to 0.2 V relative to the Ag/AgCl electrode for 10 s with oxygen flowing along the back of the electrode.

A fuel test station (FCT-2000, Electrochem) was used to measure cell polarization. Hydrogen and gases were passed through a temperature-controlled humidifiers to reflect on the separate humidifiers used for oxygen and hydrogen. The humidification temperatures of the anode and cathode gases were 358 and 343 K, with flow rates of 50 and 30 ml min^{-1}, respectively. The cell was kept at 333 K, and the gas pressure at the back of each electrode was 1 atm.

3. Results and discussion

3.1. Evaluation of electrode kinetics of oxygen reduction parameters from slow-sweep voltammetry as a function of temperature

Fig. 1 shows example voltammograms recorded for different electrodes. The observed polarization curves are far from the theoretical reversible potential, due to the poor kinetics of the reaction. The kinetics data were obtained using the Tafel equation [27]:

$$\eta = \frac{2.303RT}{\alpha n F} \log \frac{i}{i_0} \quad (1)$$

where $\eta = (E - E^0)$ is the overpotential, R the gas constant, T the absolute temperature, α the transfer coefficient, i_0 the exchange current density, n the number of electrons, and F is the Fara-

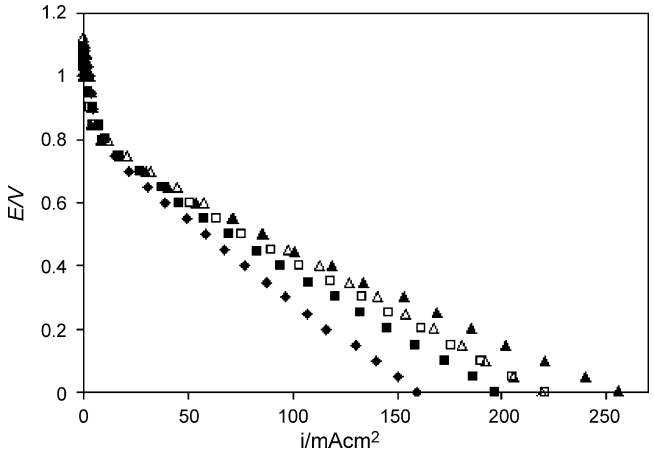

Fig. 1. Potential vs. current density for different electrodes at 25 °C and an oxygen flow rate of 30 ml min^{-1} (scan rate, 1 mV s^{-1}). Mass ratio of Vulcan/active charcoal Pt support: 0/1 (♦), 0.125/0.375 (■), 0.5/0.5 (▲), 0.375/0.125 (□), and 1/0 (△).

day's constant. All current densities in Eq. (1) were calculated relative to the real area of the working electrode. The exchange current density was calculated by extrapolating the linear portions of the Tafel plots. The theoretical reversible potential, E_r, is the standard electrode potential, E_0, for oxygen reduction (1.229 V relative to a standard hydrogen electrode at 298 K and an oxygen pressure of 1 atm) [1,28] corrected for different temperatures [1,28]. Fig. 2 shows Potential versus current density of an example electrode at various temperatures, which exhibit two well-defined linear Tafel regions. Despite the change in the Tafel slopes, the rate-determining step is the same in both the low-current-density (LCD) and high-current-density (HCD) regions [29], corresponding to the following one-electron transfer reaction:

$$O_2 + H_3O^+ + e^- \rightarrow O_2H_{(ads)}\text{–}H_2O \quad (2)$$

and hence $n = 1$ in Eq. (1). The kinetics data were obtained in both LCD and HCD regions, but the exchange current density for the HCD region varies with the thickness of the oxide layer on

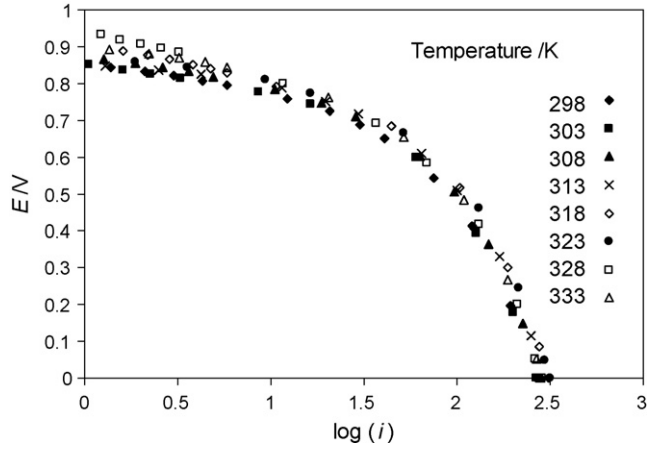

Fig. 2. Potential vs. current density for electrode with similar mass ratio of charcoal and Vulcan Pt support at different temperatures under the same conditions as in Fig. 1.

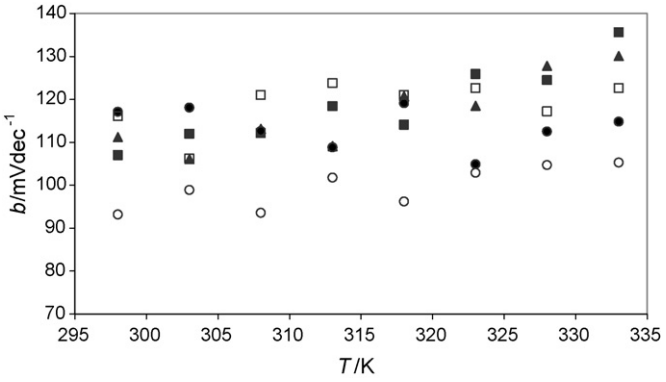

Fig. 3. Tafel slope vs. temperature for different electrodes under the same conditions as in Fig. 1. Mass ratio, of Vulcan/active charcoal Pt support: 0/1 (◯), 0.125/0.375 (■), 0.5/0.5 (▲), 0.375/0.125 (●), and 1/0 (□).

the platinum surface [30]. Therefore, kinetics data are obtained for the LCD region is more useful in comparisons.

Fig. 3 shows the Tafel slope versus temperature in the LCD region. Electrode 1 in the figure has the lowest Tafel slope, which can be attributed to the high surface area of the catalyst layer. The exchange current densities in the LCD (Fig. 4) and HCD (Fig. 5) regions show that the electrode kinetics is best in HCD electrode 3.

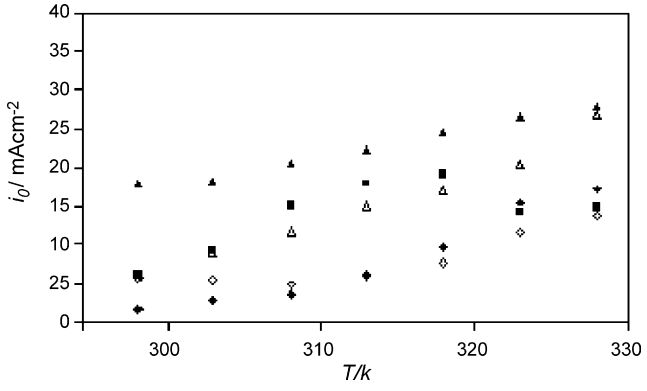

Fig. 4. HCD-region i_0 vs. temperature for different electrodes under the same conditions as in Fig. 1. Mass ratio of Vulcan/active charcoal Pt support: 0/1 (♦), 0.125/0.375 (■), 0.5/0.5 (▲), 0.375/0.125 (◯), and 1/0 (□).

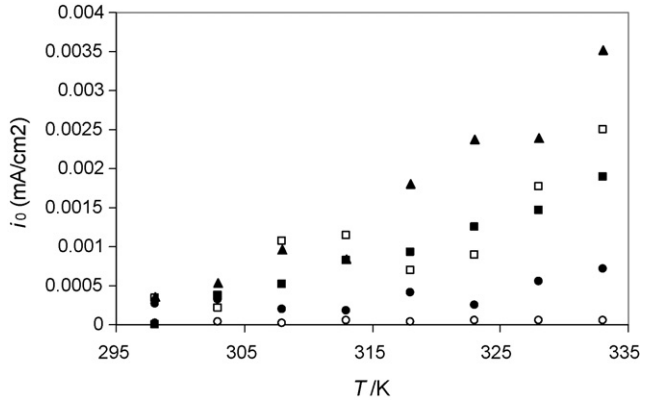

Fig. 5. LCD-region i_0 vs. temperature for different electrodes under the same conditions as in Fig. 1. Mass ratio of Vulcan/active charcoal Pt support: 0/1 (◯), 0.125/0.375 (■), 0.5/0.5 (▲), 0.375/0.125 (●), and 1/0 (□).

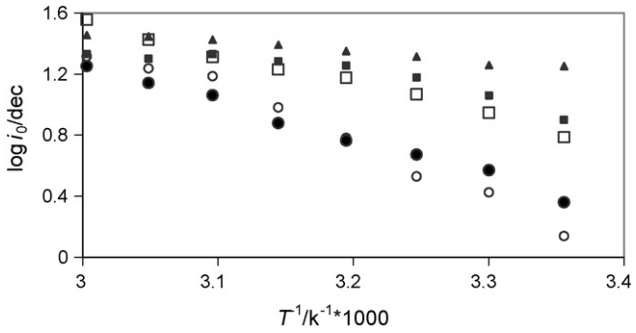

Fig. 6. Log i_0 (HCD region) vs. $1/T$ for different electrodes. Mass ratio of Vulcan/active charcoal Pt support: 0/1 (◯), 0.125/0.375 (■), 0.5/0.5 (▲), 0.375/0.125 (●), and 1/0 (□).

The activation energy was calculated from Arrhenius plots of $\log i_0$ versus T^{-1} (Fig. 6) according to the following relation [31]:

$$E_a = -2.303R\frac{d(\log i_0)}{d(1/T)} \quad (3)$$

The activation energy values from both the LCD and HCD regions are listed in Table 1, from which it is clear that the activation energy is a minimum for electrode 3 in the HCD region, implying that the kinetics of the ORR are better in this region. Moreover, this means that electrode 3 has the optimum GDE parameters in this region. Charcoal can uptake water more than Vulcan (Table 1), and decreasing the charcoal content decreases flooding in electrode; whereas decreasing the water content reduces the performance because of the reducing ionomer ion conductivity.

3.2. Chronoamperometry

The oxygen diffusion coefficients from different electrodes were determined by chronoamperometry. Fig. 7 plots I versus $t^{-1/2}$ for the oxygen reduction, which indicates the presence of the following linear relationship for different electrodes [32,33]:

$$I(t) = \frac{nFAD_b^{1/2}C_b}{(\pi t)^{1/2}} \quad (4)$$

where A is the geometric area of the electrode, D_b the diffusion coefficient, C_b the concentration of oxygen, n the number of electron in overall reaction of ORR, F the Faraday's constant, t the time and π is equal to 3.14. The equation indicates that

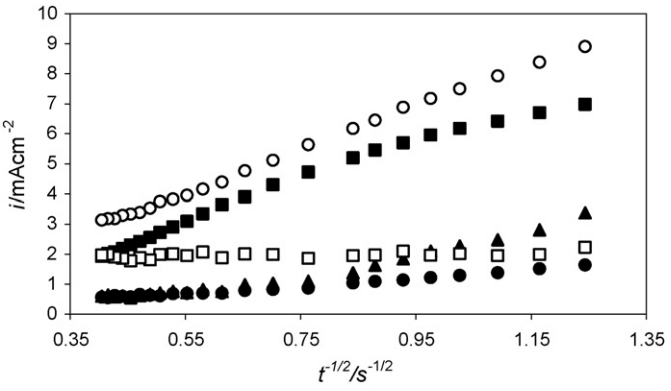

Fig. 7. Plots of i vs. $t^{-1/2}$ for oxygen reduction at different electrodes at 303 K and an oxygen pressure of 1 atm. Mass ratio of Vulcan/active charcoal Pt support: 0/1 (◯), 0.125/0.375 (■), 0.5/0.5 (▲), 0.375/0.125 (●), and 1/0 (□).

decreasing the charcoal content reduces $D_b^{-1/2}C_b$ (permeability), which implies that the oxygen permeability is higher in electrodes containing ac than in those containing VC.

3.3. Impedance diagrams

The Nyquist plots of the different electrodes obtained at different cathode potentials using EIS are shown in Figs. 8 and 9. The loop present in the low-frequency region depends on the kinetics impedance of the ORR and decreases with increasing overpotential, whereas the loop in the high-frequency region is independent of the overpotential, which indicates the impedance of the pours electrode is due to an ohmic process [34].

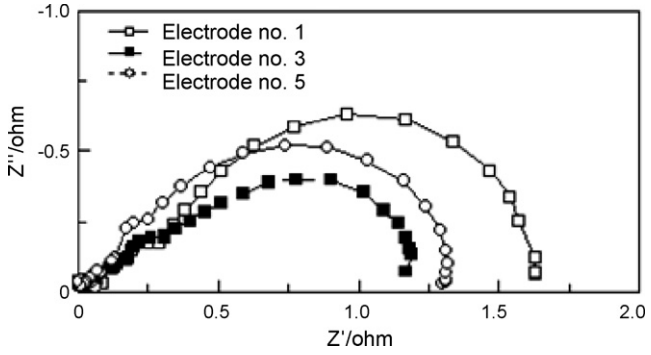

Fig. 8. Impedance spectra at a potential of 0.2 V (relative to Ag/AgCl) in the HCD region for different electrodes. Frequency range, 10 kHz–0.1 Hz. Mass ratio of Vulcan/active charcoal Pt support: 0/1 (□), 0.5/0.5 (■), and 1/0 (◯).

Table 1
Activation energy (E_{act}), water absorption, and electro active surface EAS) of various electrodes

Electrode	E_{act} in HCD region (kJ mol^{-1})	E_{act} in LCD region (kJ mol^{-1})	Permeability, $D_b^{0.5}C_b$ ($\times 10^{-11}$ mol cm^{-2} s$^{-0.5}$)	Water absorption (mg cm^{-2})	EAS (m^2 g^{-1})
1	65.8	32.6	8.63	63.4	96.1
2	21.6	74.9	8.13	55.9	84.3
3	12.4	62.6	5.57	52.9	75.2
4	47.0	24.1	3.67	53.7	61.4
5	38.9	48.0	1.42	45.7	58.1

Catalyst inks was prepared with five mass ratios using a content of Pt/VC from 0, 25, 50, 75 and 100 wt.% and that of Pt/AC in reverse (to ensure a constant total platinum loading of 0.5 mg cm^{-2}). The attained electrodes labeled by 1–5, respectively.

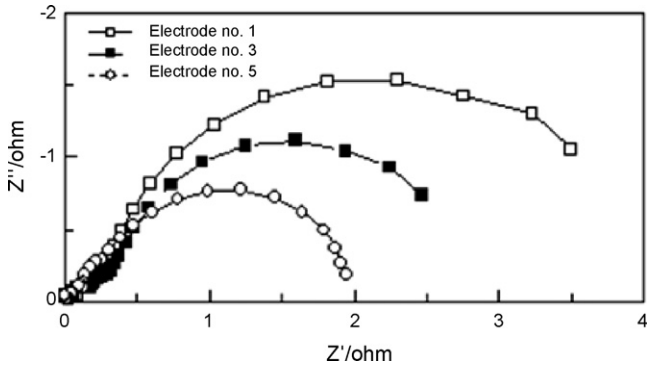

Fig. 9. Impedance spectra at a potential of 0.5 V (relative to Ag/AgCl) in the LCD region for different electrodes. Frequency range, 10 kHz–0.1 Hz. Mass ratio of Vulcan/active charcoal Pt support: 0/1 (□), 0.5/0.5 (■), and 1/0 (◯).

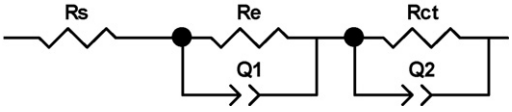

Fig. 10. Schematic representation of the equivalent circuit for the different electrodes. R_s: electrolyte resistance (subtracted from results), R_e: electrode intrinsic resistance, R_{ct}: charge transfer resistance, Q: constant-phase element.

Fig. 10 shows an equivalent circuit for the electrode process described above, where R_s is the electrolyte resistance, R_e is the electrode intrinsic resistance, R_{ct} is the charge transfer resistance, and Q_1 and Q_2 (constant-phase elements) represent the double-layer capacitances distributed between the ohmic and faradic processes, respectively [6]. The obtained parameters are listed in Table 2. The electrode resistance decreases with increasing Vulcan content, but electrode 3 has an unexpectedly low resistance, which may be due to an increase in the electronic conductance by synergism [35]; this should be evaluated in future studies. As has been shown by the Tafel parameters, the charge transfer resistance is a minimum in the LCD region for electrode 5, and electrode 3 exhibits the best kinetics in the HCD region.

3.4. Single-cell data

The polarization curves for MEAs fabricated with different electrodes are illustrated in Fig. 11. The better performance of electrode with mole ratio 50:50 confirms the above-obtained parameters, and suggests that mixing different types of carbon

Table 2
Parameters obtained from EIS diagrams with the equivalent circuit shown in Fig. 11 using nonlinear least-squares fitting (Zview, ver. 2.0)

Electrode	R_e (Ω)	R_{ct} (Ω)	
		HCD region	LCD region
1	0.615	1.076	3.501
3	0.525	0.456	2.211
5	0.594	0.840	1.385

Mass ratios of Vulcan/active charcoal Pt support are 0/1 (electrode 1), 0.5/0.5 (electrode 3), and 1/0 (electrode 5).

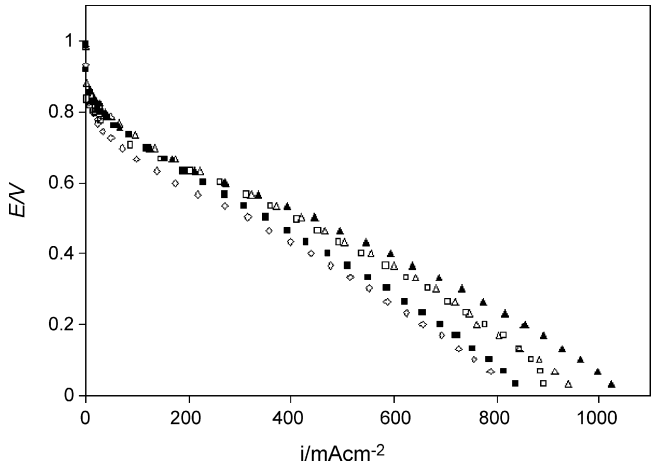

Fig. 11. MEA polarization curves. The humidification temperatures of the anode and cathode gases were 358 and 343 K, with flow rates of 50 and 30 ml min^{-1}, respectively. The cell was kept at 333 K, and the gas pressure at the back of the electrodes were 1 atm. Mass ratio of Vulcan/active charcoal Pt support for cathode: 0/1 (◇), 0.125/0.375 (■), 0.5/0.5 (▲), 0.375/0.125 (□), and 1/0 (△).

on the active surface area results in the optimal water content in the catalyst layer, and good oxygen permeability and electronic conductance. Fabricated electrode with mole ration 50:50 produces the best results for all the parameters and optimal condition for the surface area.

3.5. Scanning electron microscopy characterization

Typical scanning electron microscopy images of the electrodes are shown in Figs. 12–16. The surfaces of all the electrodes are rough and porous. The micrographs with a magnification of 250× show that increasing the activated charcoal content in the catalyst layer increases the porosity of the electrodes, which can be attributed to the electrode surface area increasing with an increasing content of fine-sized activated charcoal. This change in construction will also increase the permeability of oxygen.

Fig. 12. SEM micrograph of surface of electrode 1 (mass ratios of VC/AC is 0/1 and platinum loading is 0.5 mg cm^{-2}). recorded at 250× magnification.

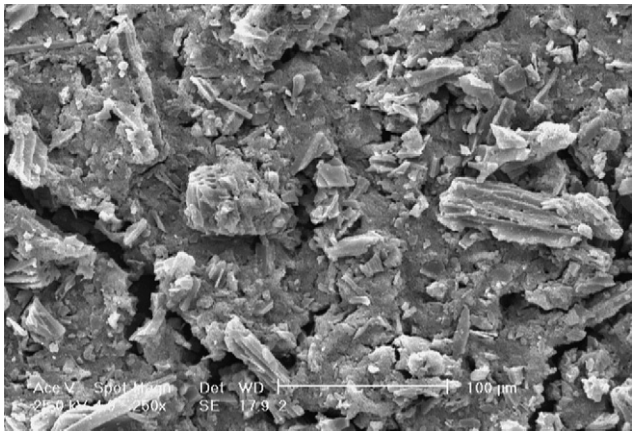

Fig. 13. SEM micrograph of surface of electrode 2 (mass ratios of VC/AC is 0.125/0.375 and platinum loading is 0.5 mg cm^{-2}) recorded at 250× magnification.

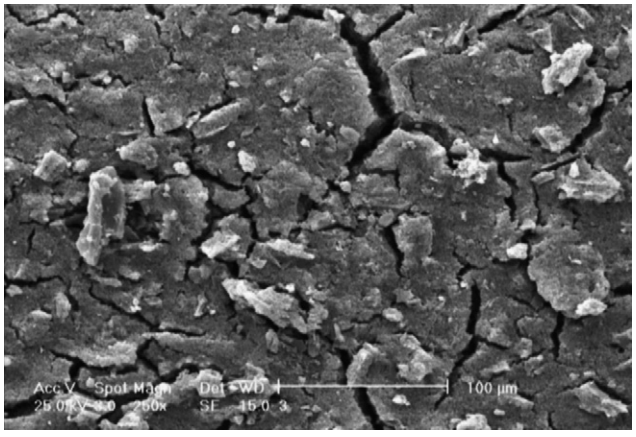

Fig. 14. SEM micrograph of surface of electrode 3 (mass ratios of VC/AC is 0.5/0.5 and platinum loading is 0.5 mg cm^{-2}) recorded at 250× magnification.

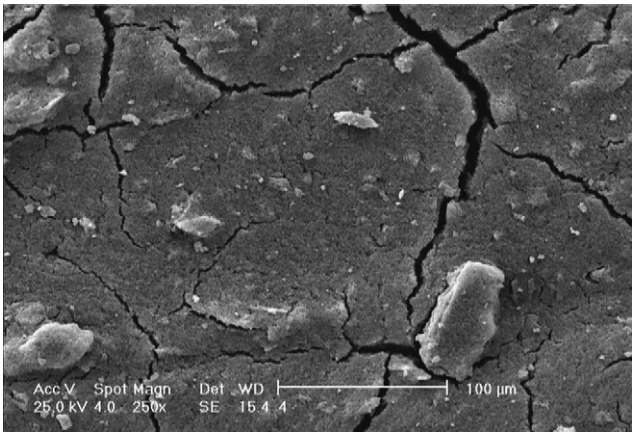

Fig. 15. SEM micrograph of surface of electrode 4 (mass ratios of VC/AC is 0.375/0.125 and platinum loading is 0.5 mg cm^{-2}) recorded at 250× magnification.

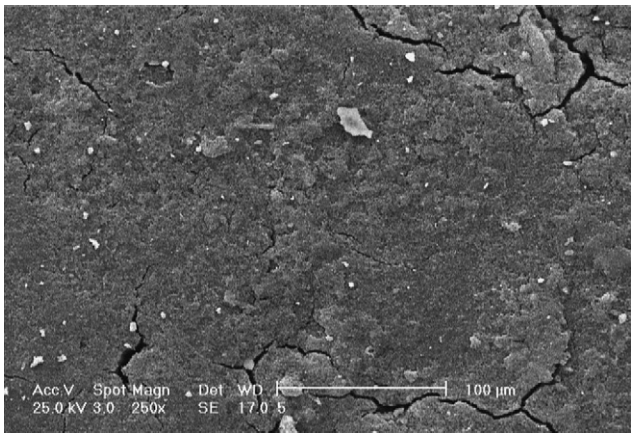

Fig. 16. SEM micrograph of surface of electrode 5 (mass ratios of VC/AC is 1/0 and platinum loading is 0.5 mg cm^{-2}) recorded at 250× magnification.

4. Conclusions

The main functions of the carbon support are to (a) disperse the ultra fine electrocatalyst particles, (b) bind strongly with the electrocatalyst particles and with the neighboring carbon support, and (c) facilitate mass transport of the reactant gases to the active sites. Having an optimized structure and composition of the active layer is vital for minimizing activation and more so, mass transport and ohmic overpotentials in the active layers. This is particularly essential for attaining the desired high power densities in PEMFCs. The electrochemical properties of GDEs based on different types of carbon black as catalyst supports have been investigated in binary support electrodes. Compared with single support electrodes, the binary electrodes exhibit improved polarization performance. The best performance is obtained in the electrode whose catalyst layer is composed of active charcoal and Vulcan XC-72R at a mass ratio of 50:50. This optimal content reduced activation energy at HCD region.

The electrode utility deteriorates when more active charcoal is present, but this increases the oxygen permeability that in turn enhances the efficiency of the GDE in the ORR. Finally, the electronic resistance of electrode is reduced by using binary support at the optimal mass ratio 50:50. It is believed that the improvement in the binary electrode is resulted from better contact between Pt and electrolyte ionomer provided by the mixture of VC and AC carbon. AC materials have different structural properties from VC. As they are mixed together with electrolyte Nafion ionomer, smaller AC particles are expected to occupy the voids inside or between agglomerates formed by larger VC particles. Therefore, the highly conductive AC particles connect the separated conductive paths, and thus the electronic conductivity of the electrode is increased.

References

[1] J. Larminie, D. Dicks, Fuel Cell Systems Explained, Wiley, 2000.
[2] E. Yeager, Electrochim. Acta 29 (1984) 1527–1537.
[3] C.A. Bassel, K. Laubernds, N.M. Rodriguez, T.K. Baker, J. Phys. Chem. B 105 (2001) 1115–1118.
[4] E. Passalacqua, P. Stati, L. Pino, M. Vivaldi, N. Giordano, E.J. Taylor, G. Wilemski, Int. J. Hydrogen Energy 17 (1992) 771–776.

[5] B. Rajesh, K. Ravindranathan Thampi, J.-M. Bonard, H.J. Mathieu, N. Xanthopoulos, B. Viswanathan, J. Power Sources 141 (2005) 35–38.
[6] S.-I. Pyun, S.-B. Lee, J. Power Sources 77 (1999) 170–177.
[7] X. Wang, I.-M. Hsing, P.L. Yue, J. Power Sources 96 (2001) 282–287.
[8] M. Watanabe, M. Tomikawa, S. Motoo, J. Electroanal. Chem. 182 (1985) 193–196.
[9] V.S. Bagotzky, A.M. Skundin, Electrochim. Acta 29 (1984) 757–765.
[10] J. Bregoli, Electrochim. Acta 23 (1978) 489–492.
[11] X. Wang, I.M. Hsing, P.L. Yue, J. Power Sources 96 (2001) 282–287.
[12] M. Maja, C. Orecchia, M. Strano, P. Tosco, M. Vanni, Electrochim. Acta 46 (2000) 423–432.
[13] M. Neergat, A.K. Shukla, J. Power Sources 104 (2002) 289–294.
[14] H. Gharibi, R. Abdullah Mirzaie, E. Shams, M. Zhiani, M. Khairmand, J. Power Sources 139 (2005) 61–66.
[15] H. Tang, J.H. Chen, Z.P. Huang, D.Z. Wang, Z.F. Ren, L.H. Nie, Y.F. Kuang, S.Z. Yao, Carbon 42 (2004) 191–197.
[16] T. Yoshitake, Y. Shmakawa, S. Kuroshima, H. Kimura, T. Ichihashi, Y. Kubo, D. Kasuya, K. Takahashi, F. Kokai, M. Yudasaka, S. Iijima, Physica B 323 (2002) 124–126.
[17] K. Tae Kim, Y. Gul Kim, J. Shik Chung, J. Electrochem. Soc. 142 (1995) 1531–1538.
[18] Z. Qi, M.C. Lefebvre, P.G. Pickup, J. Electroanal. Chem. 459 (1998) 9–14.
[19] A. Honji, T. Mori, Y. Hishinuma, K. Kurita, J. Electrochem. Soc. 137 (1998) 2084–2088.
[20] M. Sakaguchi, K. Uematsu, A. Sakata, Electrochim. Acta 34 (1989) 625–630.
[21] M. Watanabe, K. Makita, H. Usami, S. Motoo, J. Electroanal. Chem. 197 (1986) 195–208.
[22] H. Gharibi, R. Abdullah Mirzaie, J. Power Sources 115 (2003) 194–202.
[23] H. Huang, W. Zhang, M. Li, Y. Gan, J. Chen, Y. Kuang, J. Colloid Interf. Sci. 15 (2005) 593–599.
[24] L.R. Jordan, A.K. Shukla, T. Behrsing, N.R. Avery, B.C. Muddle, M. Forsyth, J. Power Sources 86 (2000) 250–254.
[25] E. Antolini, L. Giorgi, A. Pozio, E. Passalacqua, J. Power Sources 77 (1999) 136–142.
[26] V.I. Basura, P.D. Beattie, S. Holdcroft, J. Electroanal. Chem. 458 (1998) 1–5.
[27] A.J. Bard, L.R. Faulkner, Electrochemical Methods: Fundamentals and Applications, John Wiley & Sons, Inc., New York, 1980, p. 110.
[28] A.J. Bard, L.R. Faulkner, Electrochemical Methods: Fundamentals and Applications, John Wiley & Sons, Inc, New York, 1980, p. 48.
[29] P.D. Beattie, V.I. Basura, S. Holdcroft, J. Electroanal. Chem. 468 (1999) 180–192.
[30] A. Damjanovic, P.G. Hudson, J. Electrochem. Soc. 135 (1988) 2269.
[31] M.R. Tarasevich, A. Sadkowski, E. Yeager, B.E. Conway, J.O'M. Bockris, in: E. Yeager, S.U.M. Khan, R.E. White (Eds.), Comprehensive Treatise of Electrochemistry, vol. 7, Plenum Press, New York, 1983, p. 327.
[32] K. Aoki, J. Osteryoung, J. Electrochem. Soc. 125 (1981) 315.
[33] A. Pozio, M.D. Fransesco, A. Cemmi, F. Cardellini, J. Power Sources 105 (2002) 13–19.
[34] M. Ciureanu, R. Robarge, J. Phys. Chem. B 105 (2001) 3531–3539.
[35] S.E. Bourdo, T. Viswanathan, Carbon 43 (2005) 2983–2988.